J Polym Res (2013) 20:301
DOI 10.1007/s10965-013-0301-7

ORIGINAL PAPER

Dispersion of carbon nanotubes in polyamide 6 for microinjection moulding

Tânia Ferreira · Maria Conceição Paiva · António J. Pontes

Received: 7 March 2013 / Accepted: 10 October 2013

Abstract The focus of this study was to investigate the dispersion state of pure and functionalized carbon nanotubes in polyamide 6, on composites prepared by twin-screw extrusion and then processed by microinjection moulding. Nanocomposites were prepared with different carbon nanotube compositions, with and without functionalization. The nanotubes were functionalized by the 1,3-dipolar cycloaddition reaction. The dispersion of the carbon nanotube agglomerates was quantified using optical microscopy and image analysis. The effect of functionalization on the polyamide 6/carbon nanotube interface, the nanocomposite morphology and the mechanical and electrical properties were studied. It was observed that the microinjected composites with functionalized carbon nanotubes presented improved dispersion, with smaller carbon nanotube agglomerate area ratio compared to the composites with pure nanotubes. The functionalized nanotubes showed better adhesion to polyamide 6 compared to pure nanotubes, as observed by scanning electron microscopy. The incorporation of carbon nanotubes considerably improved the mechanical properties. The effect of high polymer shear rate on carbon nanotube alignment during microinjection moulding was assessed by comparing the electrical resistivity of the composite after extrusion and after microinjection moulding, through the thickness and along the flow direction. The experiments showed that the mould design and processing conditions significantly affected electrical resistivity.

T. Ferreira · M. C. Paiva (✉) · A. J. Pontes
Department of Polymer Engineering, Institute for Polymers and Composites/I3N, University of Minho, 4800-058 Guimarães, Portugal
e-mail: mcpaiva@outlook.com

M. C. Paiva
e-mail: mcpaiva@dep.uminho.pt

Published online: 24 October 2013

Keywords Carbon nanotubes · Functionalization · Dispersion · Microinjection moulding

Introduction

The investigation of polymer nanocomposites and the development of new nanostructured materials have attracted considerable interest in recent years, aiming at applications that require high performance and exceptional electrical and mechanical properties.

Carbon nanotubes (CNT) have attracted the attention of researchers in various fields such as chemistry, physics, materials science and engineering, due to their unique structure, large aspect ratio, low density, exceptional thermal and electrical conductivity, and mechanical properties [1, 2]. Several potential applications have been proposed for CNT, including those involving the production of nanocomposites with polymer matrices [3, 4]. In this area, polymer-based nanocomposites are particularly interesting, due to the ease of fabrication, the range of shapes that may be produced and the possibility of miniaturization [5].

The main challenge is to convey the excellent properties of CNT to the composites, to form electrically conductive materials with significantly enhanced mechanical properties, at low filler contents. The composite percolation threshold depends on several parameters such as the type of CNT, the matrix composition and morphology, and the filler dispersion state [1, 6].

Nanocomposite properties are limited by the ability to conveniently disperse the CNT in the polymer, forming a conductive network. The optimization of the composite's mechanical properties also depends on the ability to extensively disperse the CNT agglomerates, and to establish a strong CNT-polymer interface. The chemical inertia of the CNTs surface and weak interactions between the CNTs and most polymers are

limitations to the preparation of nanocomposites with good mechanical properties. The chemical modification of the CNT surface to improve the compatibility with the polymer is a strategy that is proving to be efficient for the enhancement of the composite's properties. For example, Li et al. [7] increased the compatibility and dispersion of multiwall CNTs in polyamide 6 (PA6) by amino-functionalization. CNT functionalization may enhance their dispersion, but its main role is expected to be the establishment of efficient load transfer from the polymer to the nanotube network [2]. Liu et al. improved the elastic modulus and yield strength of PA6 composite prepared via melt mixing and compression moulding, attributing this to good dispersion and adhesion [8]. The improvement in mechanical properties and changes in the crystallization behaviour of the PA6 composites prepared by melt compounding and microinjection moulding were associated to CNT functionalization by amidation that improved wettability and dispersion [9].

The dispersion of CNT in the polymer to the exact level required for the establishment of a CNT network with the lower CNT content possible, together with a good CNT-polymer interface, appear to be the key factors for the formation of nanocomposites with good mechanical and electrical properties. Thus, the characterization of the CNT dispersion level is important for the understanding of the nanocomposite physical and mechanical properties. The study of the agglomerate dispersion mechanisms in melt mixing reported by G. R. Kasaliwal et al. [10] provides an interpretation based on agglomerate rupture and erosion mechanisms. The authors concluded that CNT agglomerate dispersion by rupture mechanism requires less time and high shear stress, whereas at low shear stress the erosion mechanism dominates, requiring a longer time to act. Optical microscopy (OM) was used to investigate the CNT agglomerate morphology in the composites, to quantify CNT dispersion and distribution and to analyze the presence of remaining primary agglomerates, and may help to establish a relationship between structure, properties and process conditions [3].

Several processing methods such as solution mixing [11], in situ polymerization [12] and melt-mixing [13–17] have been tried to produce homogeneous dispersion of CNTs in a polymer matrix. Among these, melt mixing with thermoplastic polymers is the more convenient given its compatibility with current industrial practices, higher yield and solvent free procedure. In this area, only a small number of studies report microinjection molding (μIM) as the method of shaping the conductive polymer composites, and its influence on the composite properties [18, 19].

The process of μIM is one of the most efficient and economic processes for the large-scale production of thermoplastic polymer microparts with high precision, with the ability to produce complicated 3D parts for the miniaturization of components. This is a global trend for application in many industrial sectors: automotive, aeronautics, telecommunications, electronics, biomedical, informatics [5]. Significant work on μIM was reported along the last decade, most of it concerning neat polymers [20, 21]. The complex thermomechanical history imposed on the polymer, extreme injection pressure, high shear, elongational flow, cooling rate and very short cycle time, influence the polymer morphology [22]. When forming nanocomposite parts, these processing conditions affect the establishment of a nanotube network, and thus the nanocomposite properties. For the composite electrical properties, it was reported that the percolation threshold is usually found to be higher for thermoplastic matrices. Abassi et al. [19] concluded that the shear flow in the μIM process could induce significant CNT alignment, decreasing CNT contact, and shifting the percolation threshold to higher filler contents. They reported a percolation threshold of 9 wt. % for μIM PC/MWNT composites, compared to 3 wt. % observed for compression moulded samples. For polyamide nanocomposites the reported values of the percolation threshold were found to be in the range of 2,5-7 wt. % for melt-mixed and compression moulded films [6] and 4–6 wt. % for injection moulded samples [15].

According to theoretical investigations using Monte Carlo simulations, a minimum resistivity occurs for a partially aligned rather than for a perfectly aligned nanotube film and, when the CNT are highly aligned, the resistivity strongly depends on the measurement direction, increasing two orders of magnitude when alignment and measurement directions are not similar [23]. Recently, Mahmoodi et al. compare the electrical resistivity in the flow and thickness directions for μIM samples with different mold cavities and compression molding [24]. They concluded that μIM through an edge gate led to higher volume resistivity in the flow direction and lower in the thickness direction, compared to μIM through a fan gate.

In the present work μIM was used to produce nanocomposite specimens based on PA 6 and CNTs. The CNTs and PA 6 were melt blended by mini twin screw extrusion and processed by μIM to mold micro-size test bars. The CNTs used were as received and chemically functionalized, using a non-aggressive chemical procedure that covalently bonds pyrrolidine groups to the CNT surface [25, 26]. This procedure modifies the CNT surface without breaking or oxidizing the CNT. The influence of the processing steps on the CNT dispersion state was analyzed by OM and scanning electron microscopy. The composites were characterized in terms of the electrical conductivity and tensile properties.

Experimental section

Carbon nanotube functionalization and characterization

The CNT used were NC7000 from Nanocyl, Belgium. They were chemically functionalized using the 1,3 – dipolar cycloaddition reaction of azomethine ylides using the experimental route described in [27].

The amino acid used was *N*-benzyloxycarbonylglycine (Z-gly-OH, 99 %, from Aldrich). Paraformaldehyde (reagent grade from Sigma) was used to form formaldehyde by thermal decomposition. The reagents were blended in a 1:5 molar ratio. The mixture of reagents and CNT was suspended in a small volume of diethyl ether, sonicated during 3 min and heated in a round bottom flask until total evaporation of the solvent. Then, the mixture was heated for 3 h at 250 °C. The resulting CNT were washed with ethanol, filtered and dried. The functionalized CNT were analyzed by thermogravimetric analysis (TGA) on a TA Q500, and by X-ray photoelectron spectroscopy (XPS), on an AxiS Ultra photoelectron spectrometer.

Preparation of carbon nanotube/polyamide 6 composites

The nanocomposites were prepared by melt mixing PA6 (Badamid®B70) with 1, 1.5, 3 and 4.5 wt. % of non functionalized CNT (p-CNT) and functionalized CNT (f-CNT) on a mini twin-screw extruder. The operating variables were temperature, throughput and screw speed. The temperature profile selected was 245, 255, 255, 255 and 235 °C from feeding zone to die. The throughput was kept constant at 120 g/h.

The extruded nanocomposites were microinjection moulded using a Boy 12 A. The microinjection moulding machine has an injection screw of ∅14 mm (Dr Boy, Germany) that combines technical characteristics required for microinjection and affordability. The injection moulding cell also includes a mould temperature regulator and an external control unit for the cartridge heaters used in the temperature control system of the mould. The Boy 12 A machine is able to meter an injection volume of 0.1 cm^3 at a high flow rate, up to 15.6 cm^3 s^{-1}. The injection pressure is limited to 240 MPa.

μIM of the PA/CNT nanocomposites was carried out at a temperature profile in the injection unit ranging from 210, 220, 230, 235, 245 to 270 °C, under a pressure of 100 bar, while the speed was kept constant at 240 mm/s. The mold temperature was optimized and kept at ~100°C.

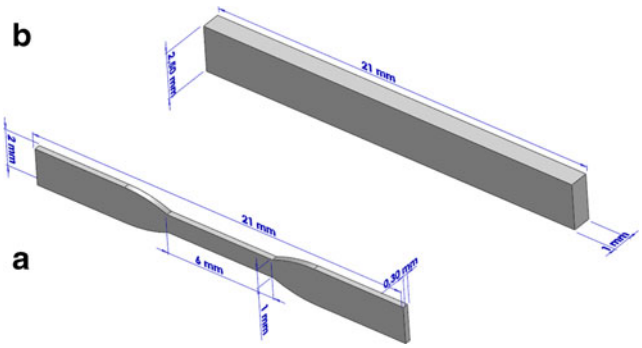

Fig. 1 Nominal dimensions of tensile (**a**) and parallelepipedic (**b**) specimens

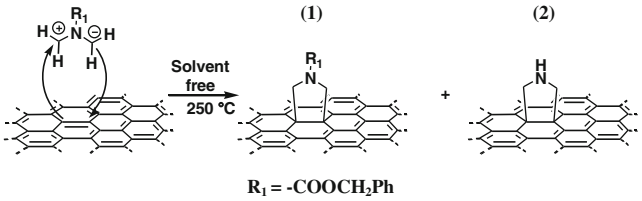

Fig. 2 Functionalization of the CNT surface using the 1,3-dipolar cycloaddition reaction

The tensile specimens were produced using a mold with the dog-bone shape cavity and dimensions described in Fig. 1a; the parallelepipedic specimens were produced using the mold shape and dimensions described in Fig. 1b.

Composite characterization

Morphology

The composite morphology was analyzed by optical and scanning electron microscopy (OM and SEM, respectively). OM observations were carried out on 5μm thickness microtomed sections of the composites, obtained with a Leitz 1401 microtome. The microtomed sections of the extruded strands were obtained perpendicular to the extrusion direction, the μIM tensile specimens were obtained along the flow direction, and the parallelepipedic specimens were obtained parallel and perpendicularly to the flow direction. The morphology of the CNT agglomerate dispersion was analyzed using an Olympus BH2 optical microscope in transmission mode. Images were acquired with a digital camera Leica DFC 280 coupled to the microscope. The CNT agglomerate area, total micrograph area and number of agglomerates were measured using the software Leica Qwin Pro. At least six micrographs of different thin sections were analysed to provide statistically significant data.

The extruded, parallelepipedic and tensile μIM samples were cryo-fractured, sputter-coated with a thin layer of palladium-gold and observed by SEM, on a FEI Quanta 400 FEG ESEM.

Electrical resistivity

The electrical resistivity of the composites was measured by the DC resistance in the flow direction, for the extruded and μIM samples. The measurements on the μIM samples were performed along the flow direction, and also across the thickness

Table 1 Nitrogen and oxygen atomic composition of CNT obtained by XPS and weight loss results measured by TGA

Sample	N (at%)	O (at%)	TGA weight loss (%)
p-CNT	–	0.8	1.6±0.7
f-CNT	2.0	1.4	16.7±1.2

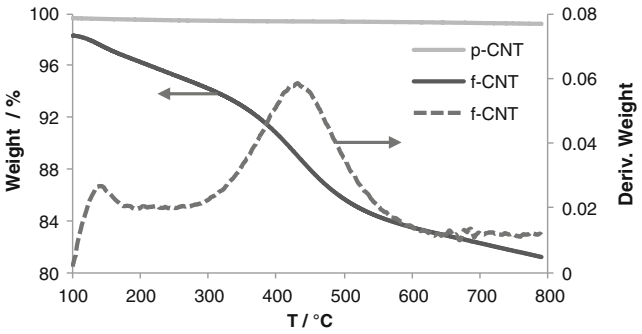

Fig. 3 Thermogravimetric analysis plots for as received and functionalized CNT, and the TGA curve derivative

for the parallelepipedic samples. For the measurements in the flow direction, samples with approximately 2–3 mm length were cut from μIM parallelepiped samples and extruded strands, while for tensile specimens the surface was polished to remove the insulating thin layer of polymer previously observed by OM. The same procedure was used for the μIM parallelepiped samples, for resistance measurements across the thickness. The contact area was coated beforehand with a thin layer of silver lacquer (Agar Scientific Batch No. O416) to ensure good contact of the sample surface with the electrodes.

The measurements were carried out at room temperature using a Picoamperimeter/voltage source Keythley 6487 equipped with a two probe test fixture. For each sample the *I-V* curves were obtained in the range of −10 V to 10 V, and the resistance was determined from the slope of the curve. The resistance was then converted to volume resistivity accounting for the sample geometry.

Mechanical properties

The tensile tests were performed on a Instron 4505 at room temperature, at a constant speed of 5 mm/min, 14 mm of gauge length, and using a load cell of 1 kN. The tensile strength, elongation at break and Young's modulus were measured. The reported values are an average over six tested specimens, for each composition and condition.

Results and Discussion

CNT functionalization and characterization

The 1,3-dipolar cycloaddition reaction was carried out using an α-amino acid and an aldeyde, under solvent free conditions, as described elsewhere [27]. The dipole formed may react with the CNT surface through cycloaddition, forming pyrrolidine groups at the CNT surface, as represented in Fig. 2. The pyrrolidine groups may establish strong interactions with the amide groups of PA6, thus it is expected to improve the CNT/PA6 interface, and the impregnation of the CNT agglomerates by the polymer. Thus, the functionalization is expected to improve the polymer/CNT interface and facilitate the CNT dispersion.

Based on a previous study [25], it was observed that the reaction may yield two products: benzyl carbamate cycloadduct (**1**) and/or pyrrolidine (**2**) on the CNT surface.

According to XPS results for as received and functionalized CNT (Table 1) and considering that the increase in N

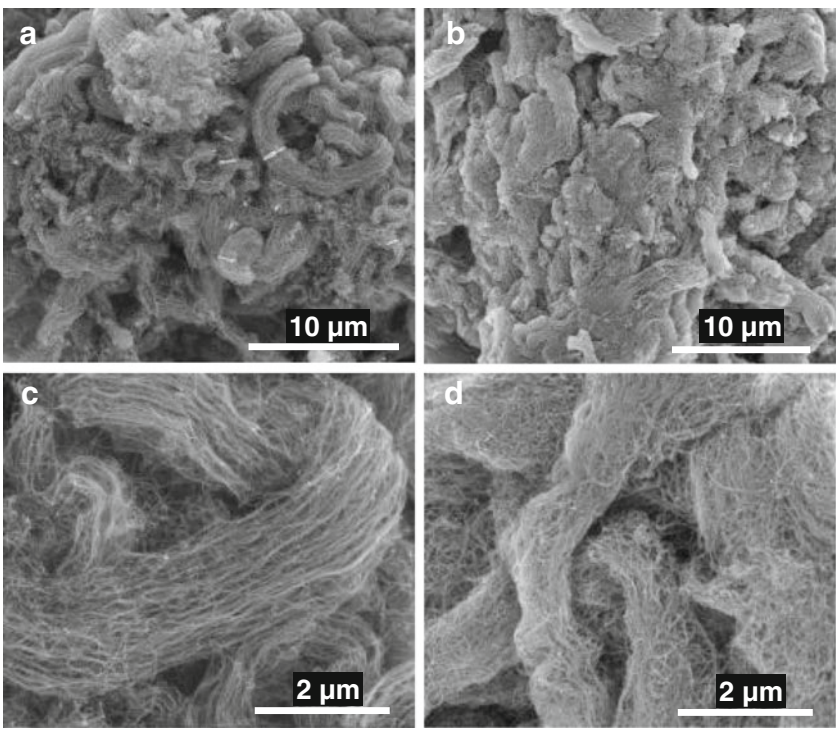

Fig. 4 SEM micrographs of as received (**a** and **c**) and functionalized (**b** and **d**) CNT

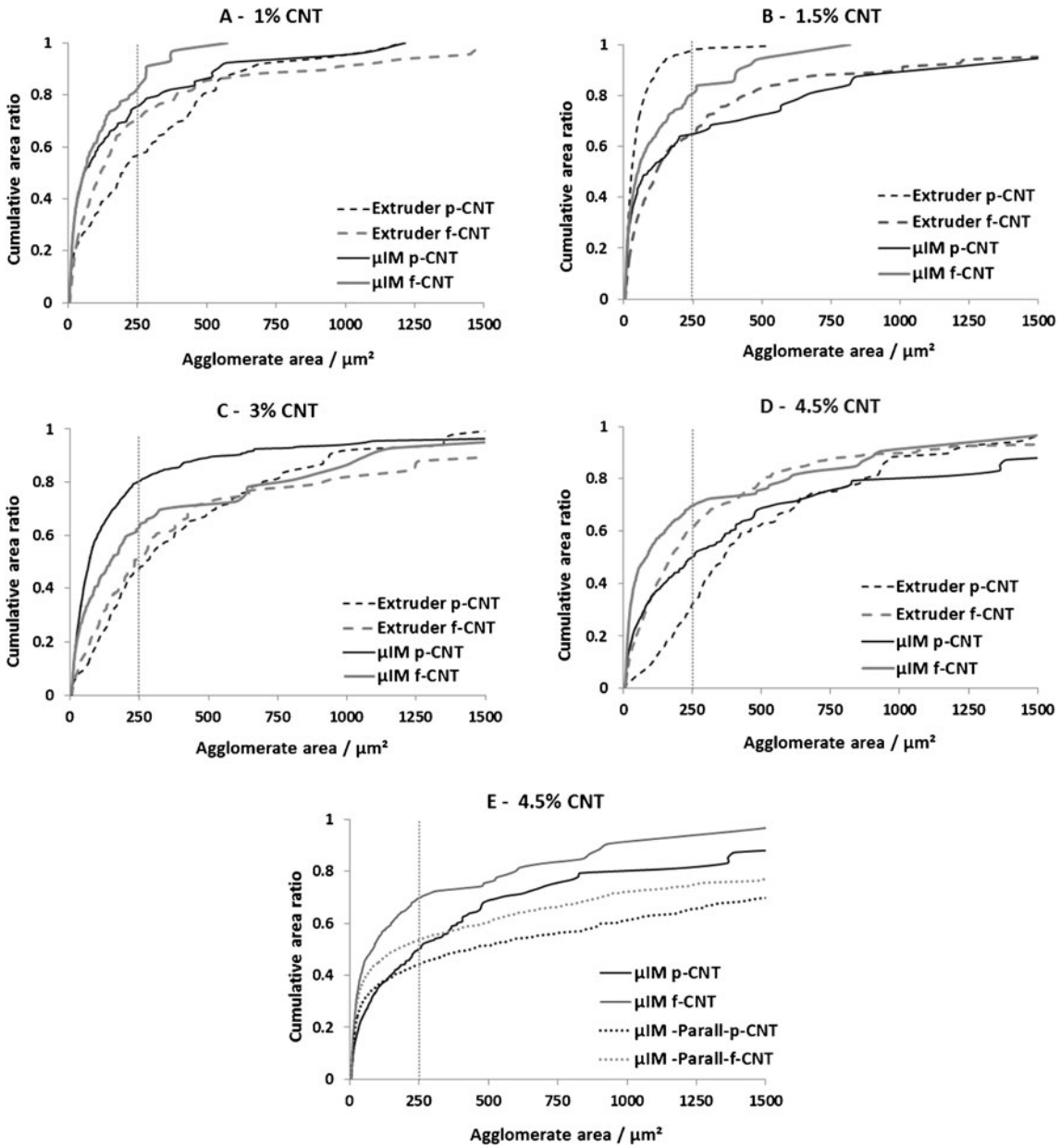

Fig. 5 **a** to **d** represent the cumulative area ratio for the composites prepared by extrusion (*dashed line*) and µIM tensile (*continuous line*); **e** compares the cumulative area ratio for the composites obtained from µIM tensile (*continuous line*) and parallelepipedic specimens (*dotted line*)

concentration is attributed to groups 1 and 2, the degree of functionalization is 2.0 % of functional groups relative to C atoms. Since the increase in oxygen concentration results from the O present in the protective group of the cyclic amine 1, the chemical composition of the functional groups was estimated to be approximately 15 % of benzyl carbamate, **1**, and 85 % of pyrrolidine, **2**.

The thermal stability of the f-CNT in dry conditions was investigated and compared to p-CNT. The corresponding TGA curves are depicted in Fig. 3 and the weight loss presented in Table 1.

The as received and functionalized CNT were observed by SEM. Figure 4 shows representative images at two magnification levels. Higher magnifications, Fig. 4c and d reveals long entangled CNT bundles, for p-CNT and f-CNT, demonstrating the mild nature of the functionalization route.

Study of carbon nanotube dispersion

OM was used to measure the area of the CNT agglomerates observed on composite sections and to assess their distribution in the polymer. The micrographs obtained by OM were analyzed, and all the CNT agglomerates with area greater than 5 μm^2 were measured. The average agglomerate area, number of agglomerates per unit area, and agglomerate area ratio defined as the ratio of the total area covered by agglomerates to the total

composite area analyzed, A_R, were determined. The variation of the cumulative agglomerate area ratio distribution, F, with the area of the agglomerates, illustrates the major characteristics of the non-dispersed CNT fraction, as explained elsewhere [26]. This representation is obtained by ranking the agglomerate areas measured, A_i, in increasing order of magnitude and plotting their cumulative area (the sum of the agglomerate areas $\sum_{i=1}^{j} A_i$, from the smaller to the jth agglomerate, divided by the total agglomerate area, $A=\sum_{i=1}^{n} A_i$) as a function of the agglomerate areas A_j. This is represented in Fig. 5 for the composites with 1, 1.5, 3 and 4.5 wt. % of p-CNT and f-CNT. The plots highlight the fraction of agglomerates with areas smaller than 250 μm^2 present in each composite. The results show that the composites obtained after extrusion under the current processing conditions presented the larger CNT agglomerates, while after μIM the fraction of small agglomerates increased considerably. The effect of CNT functionalization was, for most of the composites, to reduce the size of the CNT agglomerates.

Figure 5e compares the cumulative agglomerate area ratio for μIM composites obtained with tensile and parallelepipedic specimen molds. It was observed that the shape of the μI mold affected the CNT agglomerate size, the mold with smaller thickness (Fig. 1a) leading to the composites with smaller CNT agglomerates.

While the cumulative area ratio distributions obtained compare the morphology of the CNT agglomerates formed under the different composite processing conditions, it does not provide information about the CNT fraction that was effectively dispersed during the process. The latter may be assessed by the AR, that is inversely proportional to the dispersion level: the smaller the composite area covered with CNT agglomerates, the larger the fraction of CNTs that were effectively dispersed. Figure 6 illustrates how the different processing steps and CNT functionalization affected the AR.

Figure 6 shows that, except for the lower p-CNT composition, A_R was always larger for the extruded composites. Thus, the μIM step performed after composite extrusion improved the level of CNT dispersion. Functionalization enhanced CNT dispersion for the μIM composites, but this effect was not systematically observed for the extruded composites. For all compositions, μIM composites presented the lowest A_R values.

Optical micrographs of the nanocomposites with 4.5 wt.% of f-CNT or p-CNT revealed differences in the CNT agglomerate size, shape and number, as illustrated in Fig. 7. The CNT agglomerates in the extruded nanocomposites show a circular shape while the agglomerates in μIM samples present an elongated shape in the flow direction.

The cryo-fractured composites were observed by SEM, to monitor the dispersion of the non-agglomerated CNT. The cross-sections of the extruded and μIM composites, and in the latter case, the tensile and parallelepipedic bars, formed with p-CNT and f-CNT, were observed perpendicularly to the flow direction as illustrated in Fig. 7. The SEM micrographs showed that all the composites presented a large concentration of CNT outside the agglomerates with good CNT distribution. Comparison of the p-CNT and f-CNT composites shows that the latter have a better interface with the polymer, as evidenced by the longer p-CNT pull-out length, revealing a lower p-CNT/PA interaction.

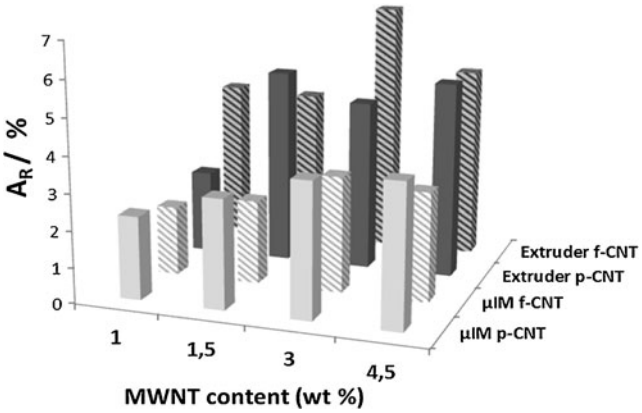

Fig. 6 Total agglomerate area ratios obtained for the composites with different CNT content

The CNT agglomerate characterization depicted in Figs. 5 and 6, and Table 2, provide important information about the differences in the dispersion mechanisms of f-CNT and p-CNT in PA 6. The extrusion process generally induced higher CNT agglomerate rupture for the f-CNT composites compared to p-CNT, generating smaller agglomerates in the former, but without considerably affecting the overall dispersed CNT fraction, leading to similar A_R (Table 2). The higher shear flow developed during μIM (relative to extrusion) lead to further enhancement of the agglomerate rupture for p- and f-CNT composites, with a greater effect on the f-CNT agglomerates. The CNT agglomerate size distribution in the polymer considerably varied with the flow geometry. The tensile bars with smaller thickness induce higher shear in the polymer melt, which enhanced the dispersion of the f-CNT and reduced their agglomerate size.

Electrical properties

The percolation threshold for PA/CNT composites is in the range of 4–6 wt. % for μIM samples [15], thus this step of our study will focus only on the 4.5 % composition.

The electrical resistivity was measured for the composites prepared by extrusion and μIM, in tensile and parallelepipedic test specimens. The measurements were performed in the direction of the flow (L) for all composites, and the parallelepipedic μIM samples were also analyzed in the perpendicular direction to the polymer flow (T). The results obtained are presented in Table 2 and Fig. 8.

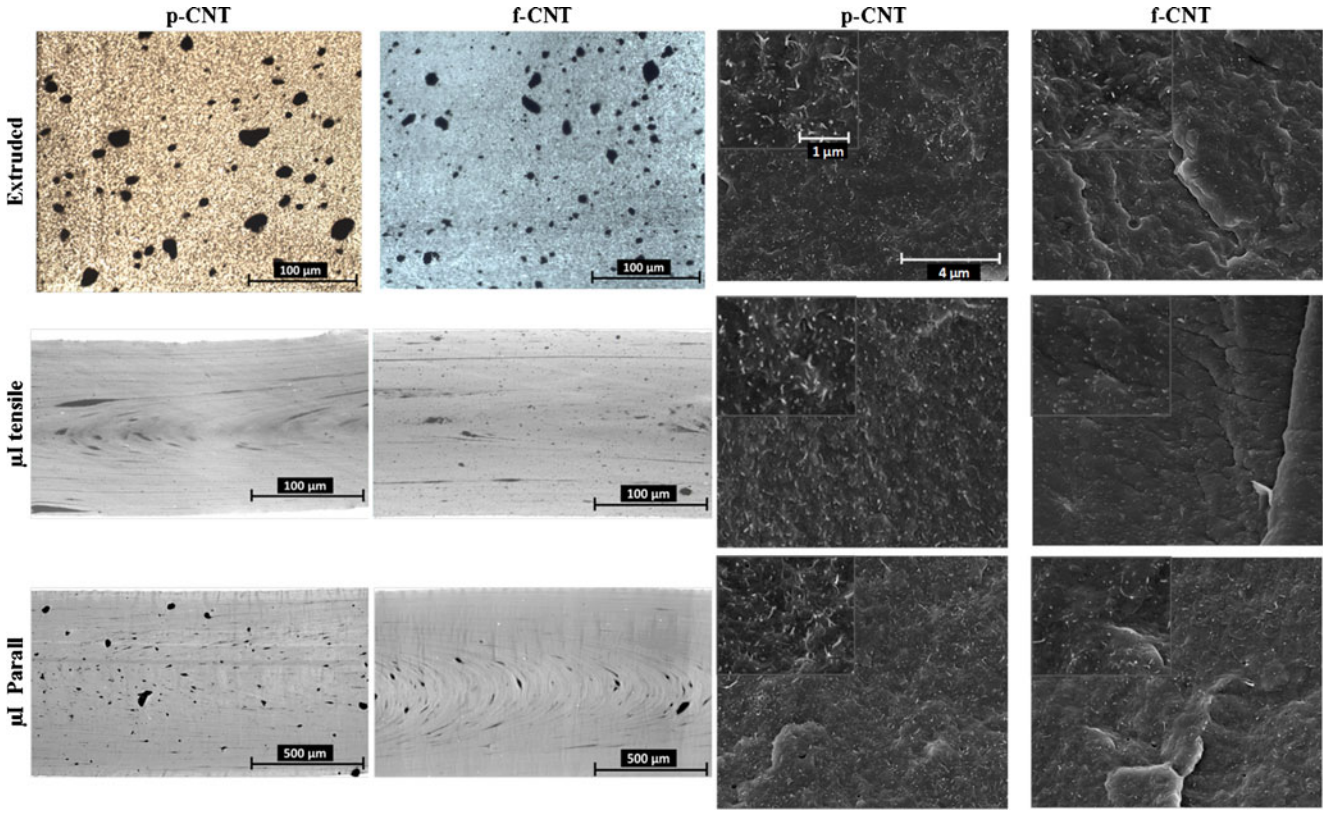

Fig. 7 OM (*left*) and SEM (*right*) micrographs of the composites with 4.5 wt.% CNT, obtained after extrusion and µIM (for tensile and parallelepipedic specimens). OM illustrates the influence of µIM on the CNT agglomerate size and shape. SEM micrographs show the CNT dispersed fraction, presenting an insert with a higher magnification image. All the SEM images have the same scale as the first

It was observed that the extruded p-CNT composites were electrically conductive, but the µIM process considerably increased the electrical resistivity of the composites, in spite of their larger fraction of dispersed CNT. Thus, it is possible that p-CNT orientation was induced by the high shear acting on the polymer melt during µIM, disrupting the CNT conductive network generated during the extrusion process. The tensile-shaped µIM specimens showed a larger increase in electrical resistivity, probably due to greater CNT orientation induced by higher polymer shear flow rate. The parallelepipedic specimens, whose electrical resistivity was measured in the L and T directions, showed lower resistivity along the flow direction (L) compared to the thickness direction (T). This type of observation is compatible with CNT alignment effects, and was described by A. Behnam et al. [23] that reported the influence of the measurement angle on the electrical resistivity of composites with aligned CNT. The improved dispersion observed for the µIM composites with p-CNT, traduced by the lower A_R and smaller agglomerates obtained compared to the extruded material, resulted in higher composite electrical resistivity.

A remarkable difference was observed for the electrical response of the composites with p-CNT and f-CNT, the former always presenting lower electrical resistivity, irrespective of the processing method. Since the functionalization alone does not affect the f-CNT electrical properties (it was demonstrated before that the electrical conductivity of f-CNT pellets was similar to that of pure CNT pellets [26]) this effect may be due

Table 2 Optical microscopy and electrical resistivity characterization of the composites with 4.5 % p-CNT and f-CNT

Sample	Processing method	Average agglomerate area (μm^2)	Number of agglomerates/μm^2	A_R	Electrical resistivity (Ω.m)
PA+4.5 % p-CNT	µIM-tensile	45	8.6×10^{-4}	3.9	7.4×10^{5}
	µIM-parall	39	7.2×10^{-4}	2.9	3.9×10^{2}
	Extrusion	146	3.7×10^{-4}	5.4	4.9
PA+4.5 % f-CNT	µIM-tensile	29	1.1×10^{-3}	3.0	2.6×10^{6}
	µIM-parall	29	1.5×10^{-3}	4.3	1.1×10^{6}
	Extrusion	55	9.7×10^{-4}	5.3	3.4×10^{8}

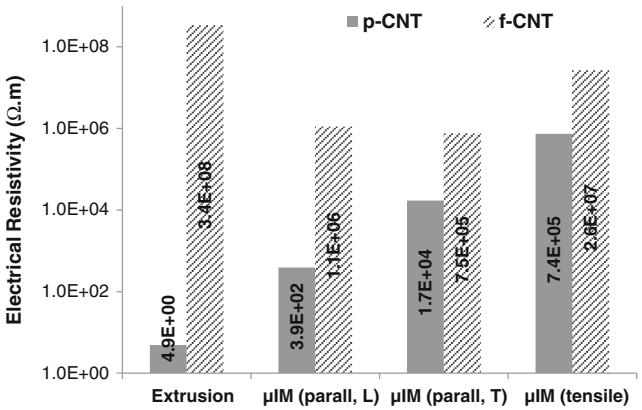

Fig. 8 Electrical resistivity of the composites prepared by the different processing methods and with different μIM molds

to the insulating action of the large polymer/f-CNT interphase formed. Nevertheless, the composites presenting higher A_R and larger agglomerate areas also show higher electrical resistivity, in opposition to what was observed for the composites with p-CNT. The electrical resistivity decreased for the μIM p-CNT composites, presenting the lower values for the parallelepipedic specimens, in the L direction. Figure 8 depicts the tendency for increase in electrical resistivity from extruded to μIM p-CNT composites, and the electrical behavior observed for the composites with f-CNT, that do not show a clear variation with the processing method.

Mechanical properties

Typical stress–strain curves of PA6 and all compositions of PA6/CNT μIM nanocomposites are shown in Fig. 9.

The elongation at break of PA increases with the incorporation of CNT (pure or functionalized), becoming much larger than the PA matrix. This result is confirmed in Fig. 10b.

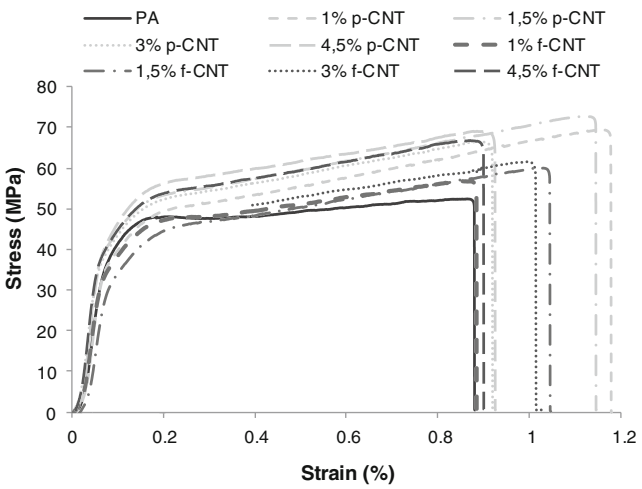

Fig. 9 Typical stress–strain curves obtained for PA6 and PA6/CNT composites

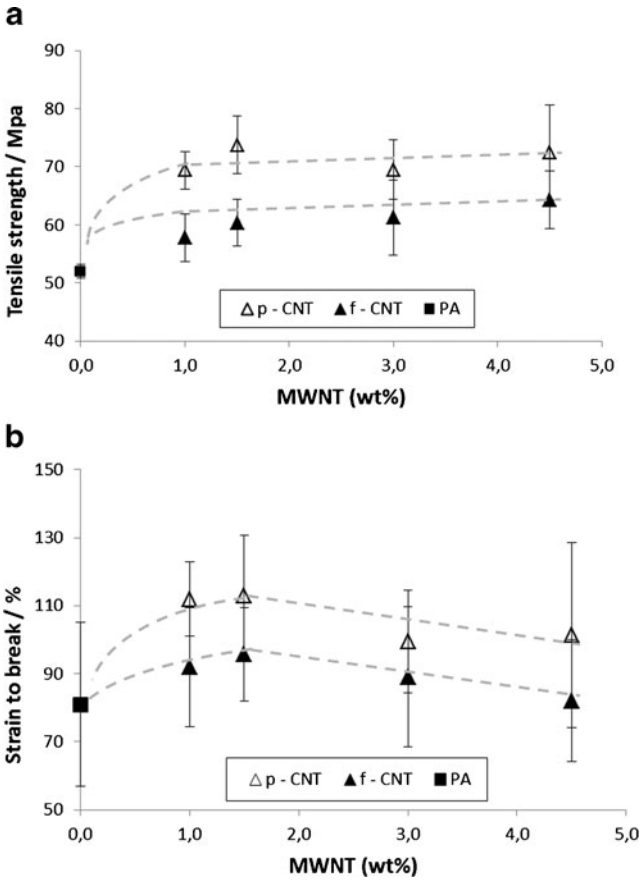

Fig. 10 Tensile strength (**a**) and strain at break (**b**) of μIM tensile-shaped specimens of PA6 and PA6/CNT samples with p-CNT and f-CNT

Figure 10a shows that the tensile strength of the nanocomposites is always greater than that of neat PA6, presenting higher values for the p-CNT composites.

Figures 10 and 11 present the tensile properties of PA6 and PA6/CNT composites, illustrating the improvement induced by the incorporation of p-CNTs and f-CNTs. The composites with p-CNT presented the best tensile properties, leading to an increase in 43 % for the modulus, relative to PA6, for the 4.5 wt.% p-CNT composites. It should be noticed that the

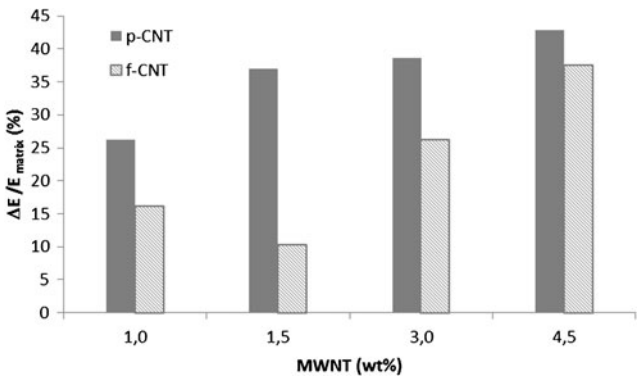

Fig. 11 Young's moduli variation for PA6/CNT composites relative to the neat polymer

incorporation of 1 % p-CNT increased the modulus by 26 % and the tensile strength by 33 %, the latter showing a similar improvement to that obtained with 4.5 wt.% of p-CNT. As reported in other works, our results also showed that the optimum tensile properties are achieved at low CNT loadings [28]. The composites with f-CNTs also presented improved tensile properties compared to PA6, but they were proportionally lower than those obtained for the corresponding p-CNT composites. This result was surprising, considering the good f-CNT wetting by PA6 observed by SEM. It may be due to the formation of thermal degradation products at the CNT/PA6 interface, since the composites were prepared at a higher temperature than the CNT functionalization temperature (270 °C versus 250 °C), or to other structural or morphological differences between p- and f-CNT composites, requiring further investigation.

Conclusions

PA6 composites with CNT, as received and functionalized, were prepared by melt blending on a mini twin-screw extruder and small specimens were produced by μIM.

The composites obtained after extrusion and μIM were characterized in terms of their morphology, measuring the CNT agglomerates size and number and observing the dispersed CNT, to contribute to the interpretation of the electrical resistivity and tensile properties results.

The composites with p-CNT showed, in general, a smaller number of larger agglomerates compared to f-CNT.

The tensile strength, elongation at break and modulus of the nanocomposites were significantly improved by the addition of CNT. The type of processing strongly affected the electrical conductivity of the nanocomposites. The specimens produced presented electrical conductivity in the semiconductor range.

Acknowledgments The authors are thankful to Fundação para a Ciência e Tecnologia for project PEst-C/CTM/LA0025/2013 (Strategic Project - LA 25 - 2013–2014), and for PhD grant for T. Ferreira (SFRH/BD/39119/2007).

References

1. Shaffer MSP, Sandler JKW (2006) In: Advani SG (ed) Processing and properties of nanocomposites. USA, World Scientific Publishing Company
2. Coleman J, Khan U, Blau W, Gun'ko Y (2006) Carbon 44:1624–1652
3. McNally T, Pötschke P (2011) Polymer-carbon nanotube composites: Preparation, properties and applications. Woodhead Publishing
4. Baughman RH, Zakhidov AA, Heer WA (2002) Science 297:787
5. Tosello G, Hansen HN (2010) In: Qin Y (ed) Micro-manufacturing engineering and technology, 1st edn. United Kingdom, Elsevier
6. Bauhofer W, Kovacs JZ (2009) Composites Science and Technology 69:1486–1498
7. Li J, Fang Z, Tong Li GA, Liu F (2007) Journal of Applied Polymer Science 106:2898–2906
8. Liu T, Phang I, Shen L, Chow S, Zhang W (2004) Macromolecules 37:7214–7222
9. Liu H, Wang X, Fang P, Wang S, Qi X, Pan C, Xie G, Liew KM (2010) Carbon 48:721–729
10. Kasaliwal GR, Pegel S, Göldel A, Pötschke P, Heinrich G (2010) Polymer 51:2708–2720
11. Qian D, Dickey EC, Andrews R, Rantell T (2000) Appl Phys Lett 76(20):2868–70
12. Yoo HJ, Jung YC, Sahoo NG, Cho JW (2006) J Macromol Sci Part B Phys 45:441–451
13. Zhang WD, Shen L, Phang IY (2004) Liu T Macromolecules 37: 256–259
14. Manchado MAL, Valentini L, Biagiotti J, Kenny JM (2005) Carbon 43:1499–1505
15. Meincke O, Kaempfer D, Weickmann H, Friedrich C, Vathauer M, Warth H (2004) Polymer 45(3):739–48
16. Schartel B, Pötschke P, Knoll U, Abdel-Goad M (2005) European Polymer Journal 41(5):1061–70
17. Pötschke P, Bhattacharyya AR, Janke A, Pegel S, Leonhardt A, Christine Täschner C, Ritschel M, Roth S, Hornbostel B, Cech J (2005) Fullerenes Nanotubes, and Carbon Nanostructures 13(1):211–224
18. Abbasi S, Derdouri, A, Carreau, PJ Proceedings of the 8th (2009) World Congress of Chemical Engineering: 2009–08
19. Abbasi S, Carreau PJ, Derdouri A (2010) Polymer 51:922–935
20. Giboz J, Coppnnex T, Mélé P (2009) J Micromech Microeng 19: 025023
21. Sha B, Dimov S, Griffiths C, Packianather MS (2007) Journal of Materials Processing Technology 183:284–296
22. Pontes AJ, Sepúlveda AT, Sampaio M, Cortez J, Cunha AM Proceedings of 24th (2008) annual meeting of the Polymer Processing Society: 2008–06
23. Behnam A, Guo J, Ural A (2007) Journal of Applied Physics 102: 044313
24. Mahmoodi M, Arjmand M, Sundararaj U, Park S (2012) Carbon 50: 1455–1464
25. Araújo R, Paiva MC, Proença MF, Silva CJR (2007) Composites Science and Technology 67:806–810
26. Novais RM, Covas JA, Paiva MC (2012) Composites: Part A 43: 833–841
27. Paiva M, Simon F, Novais R, Ferreira T, Proença M, Xu W, Besenbacher F (2010) ACS Nano 4(12):7379–7386
28. Shen J, Huang W, Wu L, Hu Y, Ye M (2007) Composites Science and Technology 67:3041–3050